IEEE Access
Multidisciplinary | Rapid Review | Open Access Journal

Received September 8, 2020, accepted September 16, 2020, date of publication September 28, 2020,
date of current version October 8, 2020.

Digital Object Identifier 10.1109/ACCESS.2020.3026820

Flexible Power-Sharing Control for Inverters-Based Microgrid Systems

SENO DARMAWAN PANJAITAN, (Member, IEEE), RUDI KURNIANTO, AND BOMO WIBOWO SANJAYA

Department of Electrical Engineering, Universitas Tanjungpura, Pontianak 78124, Indonesia

Corresponding author: Seno Darmawan Panjaitan (seno.panjaitan@ee.untan.ac.id)

This work was supported by the Directorate of Research and Community Service (DRPM), Indonesian Ministry of Research, Technology, and Higher Education (RISTEKDIKTI), under Grant PENELITIAN DASAR 2019 with contract number 101/SP2H/LT/DRPM/2019.

ABSTRACT This paper proposes a flexible method for power-sharing control of single-phase AC Microgrid or sub-system that operate inverters in parallel to supply the demand. The Photovoltaic (PV) system, coupled with batteries, energized each inverter. Solar power data from the equator city area were included in the PV system for simulation with its dynamics due to weather fluctuation. The proposed power-sharing control approach combined with integral action to improve the power quality and power-sharing accuracy. It conveys three considerations for flexible power-sharing: using virtual load voltage and the frequency at grid connection terminal (i.e., point of common coupling) in the controller without direct measurement to avoid using external communication, applying those virtual values to calculate the required parameters for an accurate power-sharing and proposing a concept of extended traditional droop control coefficient to be able to apply for various line impedances. The presented case study had two inverters supported by dynamics coupled sources from a PV system installed in an equatorial city used in the MATLAB experiment and batteries function block connected in parallel. Those inverters, located in different sub-systems, supplied two sub-systems (i.e., Microgrids) with different line impedance. The presented approach can also work for more than two or multiple sub-system scenarios by replicating the same control mechanism for the new sub-system.

INDEX TERMS Microgrid, smart grid, power-sharing control, PV systems, power electronics.

I. INTRODUCTION

Power-sharing control strategies for the microgrid system (MGS) are currently developed to cover the electricity demand that cannot be supplied by only one distributed energy resource (DER). DER is an electric power source that includes energy sources and storage that can transfer active power to the delivery facilities connected to the load(s). Numerous DER units located in neighboring sub-systems must collaboratively fulfill the demands using the excess power, instead of adding new DER(s), which is costly. A sub-system consists of DER, power interface, and area electric power system (area EPS).

One electrical type of energy resources is direct-current (DC) power that must be converted to the prerequisite power classification, either DC or AC. For AC networks or loads, inverters are commonly used to convert DC type of DER to an AC type. It is one of the main components connected directly to a DC-source DER as a power interface in an MGS. However, it has a limited output power capacity. Suppose some DERs are applied either in the same or different sub-systems to cover the demand that cannot be covered by only one inverter. In that case, it is frequently necessary to concurrently use more than one inverter to improve the system reliability, especially with priority loads. According to the standard, the converted signals should fulfill the power quality requirements such as voltage magnitude and frequency (for AC network/load) deviation, maximum total harmonic distortion (THD). Some standards or recommendations for the power quality requirements have been considered, such as IEEE 1547 [1], beside the national standards. The main issue is how to control the system to achieve those requirements as the power quality may be affected by the dynamics behavior of the DERs. The controller might implement external

The associate editor coordinating the review of this manuscript and approving it for publication was Salvatore Favuzza.

communication to get the best performance [2]–[6]. However, its technology may be costly and inflexible regarding investment and expandability. Other previous works in [7]–[23] excluded the use of external communication.

Three major power-sharing architectures are master-slave architecture, centralized control, and decentralized control. Master-slave and centralized control commonly need communication infrastructure. One of the common decentralized approaches for power-sharing is droop control. Droop control is a power-sharing technique that does not involve external communication and relies on the local measurement at the generator or electric power source.

The droop control gives advantages to system reliability and smooth integration. However, the first droop control approach should be modified to be suitable for MGS with various impedance types and load characteristics. In the beginning, it used to control the power-sharing of parallel generators based on the power drop characteristics. This method focuses on the nature in conventional distribution lines, i.e., high-voltage grid, which involves highly inductive line impedance. This method was early to control power-sharing between inverters without external communication technology in [7] by assuming that the distribution lines nature is similar to the conventional one. However, the high use of renewable energies and the continuous development in smart grids, in which MGS becomes a significant role, tends to change the system to be some sub-systems that can work independently or connected to the primary grid. The distribution line in the common MGSs becomes more resistive than the conventional electrical distribution networks, which more inductive. The distribution line distance is much shorter, and the voltage grid is much lower than the conventional one. Therefore, the first droop control method is inapplicable directly to the common MGS.

The new structure of the early method, which in the following text is called as Conventional Droop Control (CDC) method proposed in [8]–[23], considers the nature of resistive lines with or without communication technology. The boosting method [8]–[10] modifies the traditional structure of the droop method, P-ω and Q-V *droop*, to P-V *droop* and Q-ω. However, this improvement still leads to imprecise active power-sharing, limiting the applicability of the method [24]. Another modification can be seen in [11]–[13] that implements robust control using integral control to increase the sharing accuracy for active and reactive power. A problem may arise as the feedback signal uses the load voltage, which is hard to obtain because it is not locally measured, as mentioned in [24]. Another method in [14] has an effort to avoid its dependency on the information of line impedance value and various load conditions. However, its control structure may be complicated, and a high computational process is needed since the method applies an adaptive neuro-fuzzy inference system. Other approaches consider the virtual impedance method to deal with the conventional structure by modifying the resistive impedance characteristics to be more inductive [15]–[21]. In [21], this method is used for hybrid AC-DC microgrid.

Nevertheless, it needs to design carefully if the system is primarily for an islanded microgrid with a high resistive line. The large virtual inductive line impedance can severely drop the output voltage and decrease the inverters' power output capacity. This lack has also been identified in [24], regarding microgrid with high resistive line impedance.

The extended droop control approach, which maintains its conventional structure represented as P-ω and Q-V, has been proposed in [22], [23] to be applicable for a dominant resistive line impedance. The control approach in [22] considers both active and reactive currents instead of using power delivery data. However, there is no detailed explanation of its application in dominant resistive networks since the description focuses more on the inductive line, which is uncommon for MGS. The implementation of the method may work for a similar power-sharing proportion case. Its application for a different proportion may lead to inaccurate sharing. Another approach combines voltage and phase control for power-sharing in MGS, considering the dominant resistive network [23]. This method gave a good result on power-sharing accuracy, as well as voltage and frequency regulation, at a distributed generator. However, it cannot guarantee the power quality of loads, such as voltage magnitude frequency, voltage harmonic distortion, and rated-current distortion, according to its set point and the load sharing accuracy.

Our previous study in [25] introduces a preliminary approach for an accurate power/load sharing among power sources in a stand-alone MGS that maintained a good quality of power parameters. It proposes three new features developed from the traditional droop control for the dominant resistive network in an islanded MG. However, the system still considered the fixed DC source without PV system dynamics and the same line impedance.

The presented paper is the extension of the one presented in [25] to control the power-sharing between sub-systems with different DER and inverter. The DERs involve real PV data taken at the Universitas Tanjungpura area in Pontianak combined with a battery-based storage system to supply a small area EPS in MATLAB-based simulation. The real data show the electric power supply. The controller has to regulate the voltage magnitude and frequency along with the effort to maintain a high quality of harmonics level and power-sharing accuracy. A simple calculation generates the virtual load voltage and frequency with the local measurement at the interface or inverter's filter output in the power source area. Therefore, load measurement that usually needs external communication at the implementation level is unnecessary. In case the line dominant type changes, the control structure remains the same, and only modification according to the line new impedance approximation values is needed. The remaining paper will be in the following structure: the proposed idea

of the power-sharing control method, control system analysis, followed by a case study as an illustration to use the proposed method as well as its analysis result regarding the power quality recommended in [1] and power-sharing accuracy, and finally, the conclusion.

II. POWER-SHARING CONTROL

A. CDC AND ITS PREVIOUS IMPROVEMENT

In the beginning, the first droop control method has been used for power-sharing. This method assumed that the line impedance is dominantly inductive, which means a lagging power factor between the power source and load is about 90°. Its design was firstly for a grid-connected system, in which the area EPS used to connect to the primary distribution/transmission grid, with typically having a high inductive distribution line. The EPS framework (see IEEE 1547 [1]) currently tends to apply more in MGS to pave the way for a smart grid system. Hence, the droop control concept should be extended.

In MGS, the use of DERs and storage with the short distance distribution line are more common, in which the line impedance tends to be more resistive. MGS mostly uses inverters for AC loads. The power rating of each inverter may not cover the total load due to its limitation. Therefore, several inverters have to work simultaneously to be able to supply the demand. The well-known traditional droop control method for stand-alone MGS is described in [7] as active power (P) - angular frequency (w) and reactive power (Q) -voltage (V) droop relationship.

Common stand-alone MGSs, nonetheless, seem to have resistive line impedance; hence, the first droop control method is inapplicable. Thus, the efforts to develop the CDC concept can make it feasibly applied in a resistive distribution network. Some CDC developments, either using the same or different structures, can be seen in [24]. The inverter control must be precise and flexibly modified to achieve proper flexibility in power-sharing. The seamless integration of sub-systems in terms of power-sharing needs higher flexibility in control mechanisms. Therefore, the presented paper extends the previous method to have more flexibility in structure and achieve a higher degree of power-sharing accuracy and the desired power quality.

B. PLANT MODEL IN A SUB-SYSTEM

Fig. 1 shows an Electric Power System (EPS) that integrates several sub-systems, where each sub-system has its DER involving controller in it. A microgrid can apply one or more sub-systems. The term of EPS is adopted from IEEE 1547 [1]. The Point of Common Coupling (PCC) is to connect DER to the local load(s) in the sub-system during the stand-alone mode and also to the other sub-systems during sub-system/microgrid interconnected or grid-connected mode (connected to the main grid from the utility). Since the controller is distributed in each DER or sub-system, then the plant model's discussion for a sub-system is prominent

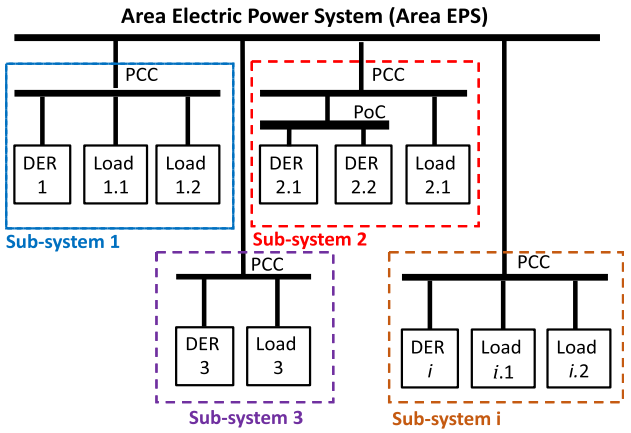

FIGURE 1. Microgrid systems are consisting of several sub-systems.

for control design. The controller should have a similar mechanism for the same type of microgrid/sub-system (ac or dc network) to ease the control design and reduce the implementation's fault.

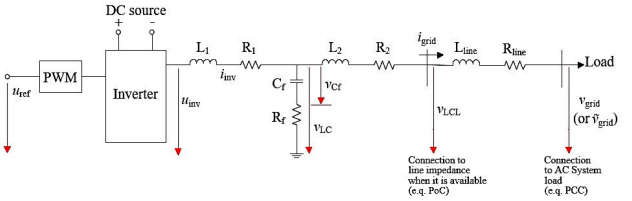

FIGURE 2. Single-phase representation of inverter, filter and line connection in a sub-system.

Fig. 2 presents the uncompensated system consisting of the Inverter system (PWM and VSC), LCL filter, and distribution line connected from the Point of Connection (PoC) to PCC. Line impedance can vary, such as a combination of R_{line} and L_{line}, dominant inductive (L_{line}) (a long-distance line from PoC to PCC with high voltage), or dominant resistive (R_{line}) (short distance line from PoC and PCC with low/medium voltage).

In our approach, we can choose either to use LCL and LC filter. For the LC filter, we can eliminate R_2 and L_2. Equation (1)-(2) shows the state-space model for the inverter, LCL filter, and line to the grid connection as a sub-system/microgrid in a stand-alone mode, while Equation (3)-(4) in on-grid mode. The output to be controlled is the sinusoidal waveform of the power interface output (i.e., V_{LC}) connected directly to the PCC voltage. Then, a sinusoidal waveform with a particular phase degree (i.e., u_{ref}) is an input of a PWM connected to an inverter as a reference for its gate signal. The controller output will provide this input value. In on-grid mode, u_{ref}, along with

v_{grid} are the inputs for the system state.

$$s\begin{bmatrix} i_{inv} \\ v_{cf} \\ i_{grid} \end{bmatrix} = \begin{bmatrix} -\frac{R_1+R_f}{L_1} & -\frac{1}{L_1} & \frac{R_f}{L_1} \\ \frac{1}{C_f} & 0 & -\frac{1}{C_f} \\ \frac{R_f}{L_2+L_{line}} & \frac{1}{L_2+L_{line}} & -\frac{R_f+R_2+R_{line}}{L_2+L_{line}} \end{bmatrix} \times \begin{bmatrix} i_{inv} \\ v_{cf} \\ i_{grid} \end{bmatrix} + \begin{bmatrix} \frac{1}{L_1} \\ 0 \\ 0 \end{bmatrix} \begin{bmatrix} u_{ref} \end{bmatrix} \quad (1)$$

$$\begin{bmatrix} v_{lc} \\ i_{grid} \end{bmatrix} = \begin{bmatrix} R_f & 1 & -R_f \\ 0 & 0 & 1 \end{bmatrix} \begin{bmatrix} i_{inv} \\ v_{cf} \\ i_{grid} \end{bmatrix} + \begin{bmatrix} 0 \\ 0 \end{bmatrix} \begin{bmatrix} u_{ref} \end{bmatrix} \quad (2)$$

$$s\begin{bmatrix} i_{inv} \\ v_{cf} \\ i_{grid} \end{bmatrix} = \begin{bmatrix} -\frac{R_1+R_f}{L_1} & -\frac{1}{L_1} & \frac{R_f}{L_1} \\ \frac{1}{C_f} & 0 & -\frac{1}{C_f} \\ \frac{R_f}{L_2+L_{line}} & \frac{1}{L_2+L_{line}} & -\frac{R_f+R_2+R_{line}}{L_2+L_{line}} \end{bmatrix} \times \begin{bmatrix} i_{inv} \\ v_{cf} \\ i_{grid} \end{bmatrix} + \begin{bmatrix} \frac{1}{L_1} & 0 \\ 0 & 0 \\ 0 & -\frac{1}{L_2+L_{line}} \end{bmatrix} \begin{bmatrix} u_{ref} \\ v_{grid} \end{bmatrix} \quad (3)$$

$$\begin{bmatrix} v_{lc} \\ i_{grid} \end{bmatrix} = \begin{bmatrix} R_f & 1 & -R_f \\ 0 & 0 & 1 \end{bmatrix} \begin{bmatrix} i_{inv} \\ v_{cf} \\ i_{grid} \end{bmatrix} + \begin{bmatrix} 0 & 0 \\ 0 & 0 \end{bmatrix} \begin{bmatrix} u_{ref} \\ v_{grid} \end{bmatrix} \quad (4)$$

C. CONTROL APPROACH FOR A SUB-SYSTEM

A sub-system presented in Fig. 2 should have its independent control scenario, especially when it is off from the primary grid (i.e., stand-alone mode). The controller must work properly when the MGS is in this mode because it is not like an on-grid feature where the utility drives voltage and frequency regulation. The control should deal with the dynamics of energy sources and also the load at the same time. Mostly Proportional-Integral (PI) control is used for this purpose. Our extended method for single DG in a microgrid, considering the load and DC source dynamics using Integral-Proportional Derivative (I-PD) and Fuzz-PI based controller, can be seen in [26]–[28]. However, the approaches have not considered the power-sharing mechanism yet.

D. THE PROPOSED POWER-SHARING CONTROL APPROACH BETWEEN SUB-SYSTEMS

The concept for power-sharing that considers the modification of traditional droop control using the fixed-rate of DC source in a stand-alone mode is in [25]. It has not yet been considered using real PV data combined with battery in the simulation results.

The presented paper considers using real PV data combined with battery in the simulation and proposes a flexible method for proportional power-sharing between the sub-systems. The proposed control deals with voltage and frequency regulation with accurate power-sharing among sub-systems. It simplifies the previous work presented in [25] by using only one power-sharing coefficient for each voltage and frequency control feedback. Each sub-system has a flexible and formal control mechanism once it is connected or disconnected to other sub-systems, either work in sharing or stand-alone mode. Furthermore, it can also work either in stand-alone or grid-connected mode.

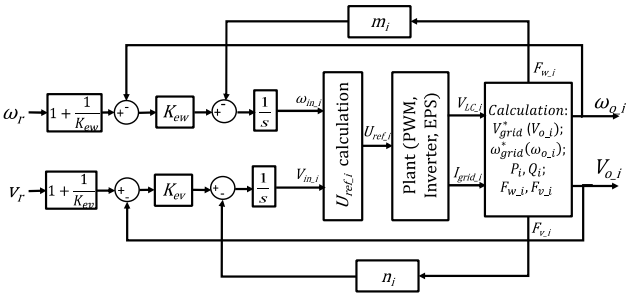

FIGURE 3. Block diagram of the proposed power-sharing control in Sub-system *i*.

Fig. 3 shows a block diagram of the proposed control method, where each controller is located in DER in each sub-system. Therefore, the i-th parameter in the equations of the proposed method is related to the i-th controller. The universal constant (without i index) will be set the same for all controllers. Reference and actual angular frequency are represented as ω_r and ω_{o_i} respectively, while V_r represents the rated voltage in RMS and V_{o_i} is the voltage on the output terminal, either PoC (in case MGS does not have a distribution line) or PCC in a stand-alone state. In on-grid mode, the utility drives the PCC voltage. Therefore, the regulation of V_{o_i} will drive grid current (I_{grid_i}) flowing through the MGS (i.e., sub-system). The i-th sub-system represents the subsystem's number and their specific parameters, while the variables and gain without the i-th number are constant with the same values in all sub-systems.

F_{w_i} and F_{v_i} represent the power values calculated based on the measured grid current in sub-system i (I_{grid_i}), calculated RMS grid voltage, and the impedance, shown in Equation (5) and (6). Those values are used to generate power-sharing parameters for the phase difference and voltage regulation accordingly. In resistive dominant impedance line, F_{w_i} will be strongly affected by the reactive power value and F_{v_i} by the active power. The dominant resistive line is common cases in stand-alone MGS, where a particular controller independently controls the power. The controller is located modularly in each MGS. In contrast, in the system where the power supply is dominated by the utility with a high voltage transmission line, the distribution line becomes more inductive. In this case, F_{w_i} will be strongly dominated by the reactive power, while F_{v_i} by the active power.

$$F_{w\_i} = \frac{X_{2\_i} + X_{line\_i}}{Z_{2\_i} + Z_{line\_i}} P_i - \frac{R_{2\_i} + R_{line\_i}}{Z_{2\_i} + Z_{line\_i}} Q_i \quad (5)$$

$$F_{v\_i} = \frac{R_{2\_i} + R_{line\_i}}{Z_{2\_i} + Z_{line\_i}} P_i + \frac{X_{2\_i} + X_{line\_i}}{Z_{2\_i} + Z_{line\_i}} Q_i \quad (6)$$

Calculation of voltage references (U_{ref_i}) for the PWM, which subsequently determines the gate signal for inverter, are formulated in Equation (7) and (8). For highly dominant resistive line impedance (the impedance between V_{LC} and V_{grid}), $m_i F_{w\_i} \approx -m_i Q_i$ and $n_i F_{v_i} \approx n_i$Pi, while in highly dominant inductive line impedance, $m_i F_{w\_i} \approx m_i P_i$ and $n_i F_{v\_i} \approx n_i Q_i$. In the case of the line impedance is a highly dominant capacitive, then $m_i F_{w\_i} \approx -m_i P_i$ and $n_i F_{v_i} \approx -n_i$Qi due to the negative value of the reactance. The reference of angular frequency (ω_r) at PCC should be determined, where this point is the closest connection to the common grid that is connected to the loads (see Fig. 1 – 2). The actual angular frequency at PCC (ω_{grid}) is calculated since it may be located in a long distance from the power interface. Thus, the local measurement cannot be done, and the communication technology requirement cannot be avoided, which will bring another cost. The virtual or calculated angular frequency at the i-th terminal (ω^*_{grid}) of the grid connection to the load is called ω_{o_i}. Similarly, the voltage reference of the output terminal is represented as v_r and the i-th actual output voltage (v_{grid}) is calculated and expressed as V^*_{grid} or V_{o_i}, which is the virtual output voltage.

$$s\omega_{in\_i} = \omega_r - m_i F_{w\_i} + K_{ew}\left(\omega_r - \omega_{o\_i}\right) \quad (7)$$
$$sV_{in\_i} = V_r - n_i F_{v\_i} + K_{ev}\left(V_r - V_{o\_i}\right) \quad (8)$$

In steady-state condition, $s\omega_{in\_i} = 0$ and $sV_{in\_i} = 0$, then from Equation (7) and (8), we can get the value of m_i and n_i by replacing F_{w_i} and F_{v_i} with the maximum apparent power (S) that has to be shared with all loads, as shown in Equation (9) and (10), respectively. The previous references mostly use the maximum power source to calculate the m_i and n_i, but it leads to unproportioned load sharing. Ensuring the total power from the integrated distributed energy sources is more than the determined maximum load demand will accurately share the power according to the proposed approach. More details about this motivation are described in [25].

$$m_i = \frac{\omega_r - e_w K_{ew}}{s} \quad (9)$$
$$n_i = \frac{v_r - e_v K_{ev}}{s} \quad (10)$$

To get the value of m_i and n_i, the required phase error (e_w) and RMS voltage error (e_v) must be determined as part of system requirements. We need to know the value of line impedance to determine the maximum active and reactive power of the load network for value P_i and Q_i. If we have two inverters and the same sharing proportion, then m_1(Sub-system 1) equals m_2 (Sub-system 2). If we require Sub-system 1 to supply double power ($P_1 = 2P_2$ and $Q_1 = 2Q_2$) than Sub-system 2, then $m_2 = 2\ m_1$. It is similar for setting n_i.

III. CONTROL SYSTEM ANALYSIS

Microgrid stability is an essential aspect of having high reliability. However, there are several levels and focuses in a microgrid that makes it more complicated to obtain the whole mathematical model for sub-systems or even system level and investigate the stability and other control analysis for state-space models, such as controllability and observability. In [29], the stability analysis is divided into two categories: an electric machine and converter stability while the stability analysis divers into two techniques: large-perturbation and small-perturbation analysis. In the presented paper in the following discussion, the control analysis is categorized based on the functionalities: power interfaces' performance in sub-systems and the power-sharing precision.

A. SUB-SYSTEM'S INTERFACE STABILITY

The system's interface is the conversion of U_{ref} to V_{LC} consisting of the inverter with its signal reference and filter (either LC or LCL). Equation (1)-(2) presents the mathematic model in a state-space of this interface. For instance, the state-space is for islanded MGS with the various values used in the case study (Table 1 in Section IV) has three eigenvalues for various line dominant impedances: (1) L-impedance (−11,007, 0, and −1,031) when $R_{line} = 0\ \Omega$ and $L_{line} = 0.01$ mH; (2) R impedance (−11,203, 40, and −1,014) when $R_{line} = 1\ \Omega$. and $L_{line} = 0$ mH; and (3) RL impedance (−11,184, −40, and −1,014) when $R_{line} = 1\ \Omega$ and $L_{line} = 0.01$ mH. The parameter values of the system in Table 1 may be different from other systems. The sub-system interface is stable either for transfer function v_{LC}/u_{ref} or i_{grid}/u_{ref}, as we can see in the root locus plot in Fig. 4. The sub-system interface is also completely state and output controllable.

B. SUB-SYSTEM STABILITY IN SHARING POWER

Power-sharing involves interconnection among sub-systems as power sources that work together to supply the demand. This sharing mechanism is not just to make sure whether the power quality fulfills the requirements, but also to achieve an accurate power-sharing among the sub-systems. Equation (11)-(12) represent a state-space model of Equation (5)-(8) with more details. The dynamics of errors formulate the disturbance of the i- th sub-system (d), such as $K_{ew}e_w$ or $K_{ew}(w_r - w_{o\_i})$ for angular frequency error dynamics (d_{1i}) and $K_{ev}e_v$ or $K_{ev}(V_r - V_{o\_i})$ for the voltage error dynamics (d_{2i}).

$$s\begin{bmatrix}\omega_{in_i}\\ v_{in_i}\end{bmatrix} = \begin{bmatrix} -m_i\left(\frac{L_{2_i}+X_{line_i}}{Z_{2_i}+Z_{line_i}}\right) & m_i\left(\frac{R_{2_i}+R_{line_i}}{Z_{2_i}+Z_{line_i}}\right) \\ -n_i\left(\frac{R_{2_i}+R_{line_i}}{Z_{2_i}+Z_{line_i}}\right) & -n_i\left(\frac{L_{2_i}+X_{line_i}}{Z_{2_i}+Z_{line_i}}\right)\end{bmatrix} \times \begin{bmatrix}P_i\\ Q_i\end{bmatrix} + \begin{bmatrix}1 & 0\\ 0 & 1\end{bmatrix}\begin{bmatrix}w_r\\ v_r\end{bmatrix} + \begin{bmatrix}d_{1i}\\ d_{2i}\end{bmatrix} \quad (11)$$

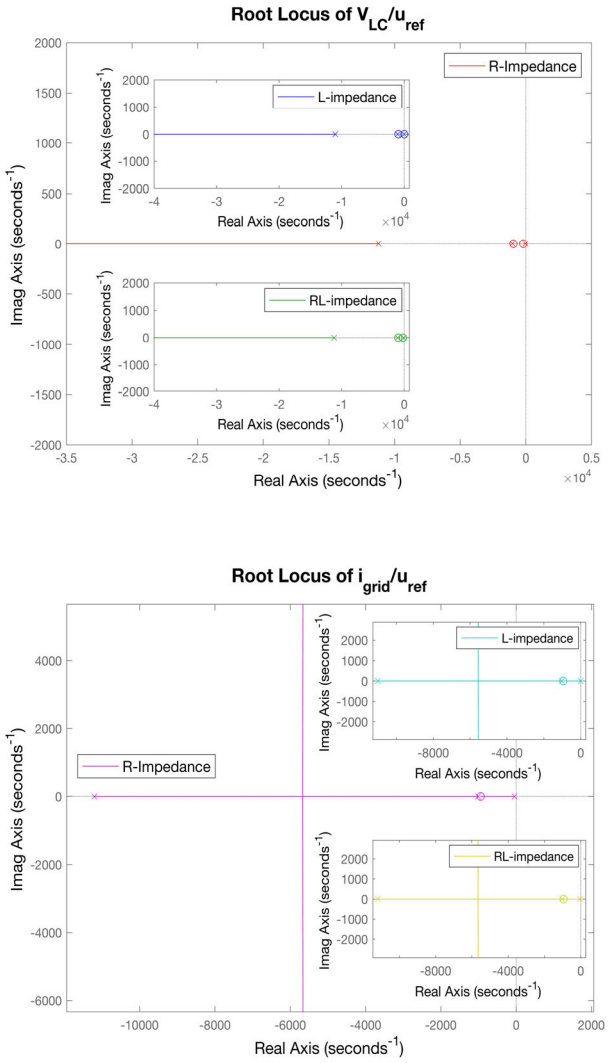

FIGURE 4. Root Locus plot of transfer function V_{LC}/u_{ref} and i_{grid}/u_{ref} (in Fig. 2) with various line impedance.

$$\begin{bmatrix} \omega_{o\_i} \\ v_{o\_i} \end{bmatrix} = \begin{bmatrix} -\frac{m_i}{K_{ew}}\left(\frac{L_{2_i}+X_{line_i}}{Z_{2_i}+Z_{line_i}}\right) & -\frac{m_i}{K_{ew}}\left(\frac{R_{2_i}+R_{line_i}}{Z_{2_i}+Z_{line_i}}\right) \\ -\frac{n_i}{K_{ew}}\left(\frac{R_{2_i}+R_{line_i}}{Z_{2_i}+Z_{line_i}}\right) & -\frac{n_i}{K_{ew}}\left(\frac{L_{2_i}+X_{line_i}}{Z_{2_i}+Z_{line_i}}\right) \end{bmatrix} \times \begin{bmatrix} P_i \\ Q_i \end{bmatrix} + \begin{bmatrix} \frac{1+K_{ew}}{K_{ew}} & 0 \\ 0 & \frac{1+K_{ew}}{K_{ew}} \end{bmatrix} \begin{bmatrix} w_r \\ v_r \end{bmatrix} \quad (12)$$

IV. CASE STUDY WITH PV DATA MONITORING

A. DESCRIPTION OF THE SYSTEM

Fig. 5 shows a schematic diagram of a power-sharing system consisting of two sub-systems used as a case study. The priority task is to achieve the power quality according to the IEEE recommendation and a very accurate power-sharing by controlling the sub-systems. Each sub-system has its controller with the same control mechanism, DER with energy source (ESO) and energy storage (EST), inverter with the filter (LC or LCL), and the local load network, that may vary

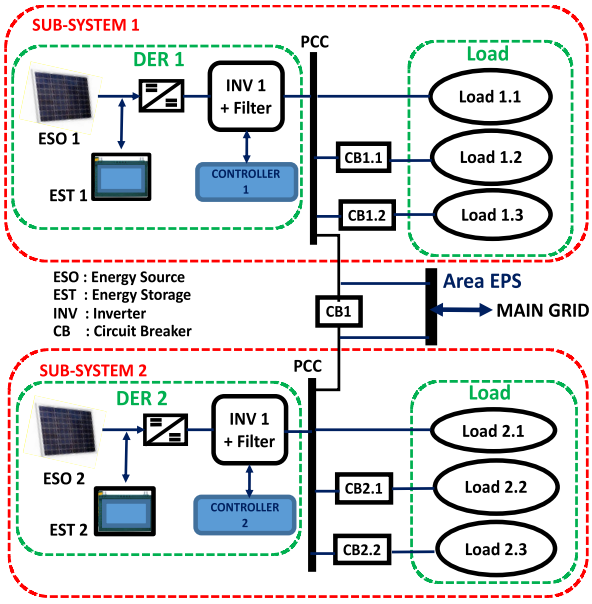

FIGURE 5. AC Microgrid system with two sub-systems as a case study including DERs, Load, and the area EPS.

depending on the system's dynamics (e.g., connection time). The sharing mechanism includes the other sub-system's load dynamics when several sub-systems operate in parallel and the desired power-sharing proportion for each sub-system.

A sub-system that is not connected to the main grid (i.e., stand-alone mode) must have independent control to ensure the desired power quality at the PCC during the power-sharing scenario. The distributed controllers located in each sub-system need to work in a particular mechanism to fulfill all sub-systems' power quality requirements.

Table 1 provides information on the system's parameters described in Fig. 5 as a case study in this paper. A DER in the system basically can work independently or collaboratively with other DER, where the power to supply the demand can be delivered from each sub-system or through a power-sharing scenario.

In the presented paper, each controller located in each sub-system, but the constant values for all the inverters involved in the sharing are the same, such as voltage and frequency reference, and error gains. For power-sharing/droop control coefficients, the value will be the same if the sharing proportion, otherwise they are different according to the proportion. The status of the circuit breakers (CBs) determines whether the system is in sharing or non-sharing mode. The connection between ESO and EST has two modes: DC-DC coupled and DC-AC coupled. The presented system used the first mode. In the implementation, the DER voltage should be about 30% of the rated voltage (i.e., 220 Vrms) and the DC-DC converter is needed to regulate the voltage to the DC-link voltage.

B. THE SYSTEM WITH PV DATA MONITORING AND INTERCONNECTION SCENARIOS

Fig. 6 shows the monitoring system based on a microcontroller (i.e., Arduino) and voltage-current sensors built to

TABLE 1. List of parameters.

Elements	Notation	Details
DER 1	ESO 1	PV array (4 Series x 10 parallel modules), each module has Pmax 125 W, Vmp 17.8 V, Imp 7.023 A, Voc 21.36 V, Isc 7.444 A, maximum system voltage 1,000 V.
	EST 1	Lithium Ion, Nominal Voltage 48 V, Rated capacity 140 Ah, Initial State of Charge 90%.
DER 2	ESO 2	PV array (4 Series x 15 parallel modules), each module has Pmax 125 W, Vmp 17.8 V, Imp 7.023 A, Voc 21.36 V, Isc 7.444 A, maximum system voltage 1,000 V.
	EST 2	Lithium Ion, Nominal Voltage 48 V, Rated capacity 150 Ah, Initial State of Charge 85%.
Interface 1	INV 1	IGBT 2 arms
	PWM 1	Single-phase full-bridge (4 pulses)
	Filter 1	Rl = 0.001 Ω, L1 = 20 mH, Cf=22 μF, Rf=48.2288 Ω, R2 = 0.0001, L2 = 5 mH
Interface 2	INV 2	IGBT 2 arms
	PWM 2	Single-phase full-bridge (4 pulses)
	Filter 2	Rl = 0.001 Ω, L1 = 20 mH, Cf=22 μF, Rf=48.2288 Ω, R2 = 0.0001, L2 = 5 mH
CB	CB switching times	Switching times: CB 1 (2s ON, 10s OFF), CB1.1 (4s ON, 10s OFF), CB 1.2 (8s ON, 10s OFF), CB 2.1 (6s ON, 10s OFF), CB 2.2 (8s ON, 10s OFF)
Impedance line	Line 1	Rg1 ≈ 0 Ohm, Lg1 = 0.01 mH
	Line 2	Rg2 = 1 Ohm, Lg2 = 0.01 mH
Load	Load 1.1	2.5 kW, 200 VAR (Q_L), 50 VAR (Q_C)
	Load 1.2	750 W, 75 VAR (Q_L), 25VAR (Q_C)
	Load 1.3	1.3 kW, 50 VAR (Q_L), 25 VAR (Q_C)
	Load 2.1	2 kW, 150 VAR (Q_L), 50 VAR (Q_C)
	Load 2.2	750 W, 75 VAR (Q_L), 25 VAR (Q_C)
	Load 2.3	600 W, 50 VAR (Q_L), 25 VAR (Q_C)

FIGURE 6. Developed monitoring system to collect data from PV system.

record the required data from PV systems. The sensors previously were calibrated in the laboratory before being used for measurement by comparing it to the standard electrical measurement tool. The monitoring data was from a PV array module placed on the Electrical Engineering Laboratory's rooftop, Universitas Tanjungpura, Pontianak. In the simulation, one-week data from a 125 Wp solar panel had been multiplied to some number of modules with the same power characteristic as the case for a larger size of a PV-system as detailed in Table 1. Power calculation from field V-I measurement for one day (24 hours) and seven days (24 hours × 7) for one module are shown in Fig. 7(a) and (b) respectively.

The Simulation followed these scenarios:

1. At 0 – 2s, Sub-system 1 and Sub-system 2 had their local load, 2.5 kW/150 VAR (Load 1.1. in TABLE 1) and 2 kW/100 VAR (Load 2.1) respectively without power-sharing,
2. At 2 - 4s, both sub-systems were connected with 2:1 power-sharing proportion, where Sub-system 1 supplied double power than Sub-system 2,
3. At 4 – 6s, more load (Load 1.2) were connected to be 5.25 kW/300 VAR in total with the same sharing proportion,
4. At 6 – 8s, Load 2.2. was connected and the total load increased to 6 kW/350 VAR,
5. At 8 – 10s, Load 1.3 and Load 2.3 were connected which increase the total sharing load to 7.8 kW/400 VAR in total,
6. At 10 – 12s, the power-sharing switch was disconnected where each Sub-system 1 and Sub-system 2 were connected to load with the same scenario at 0 – 2s.

Based on recommendations in [1], when DER is connecting to EPS, then the following recommendation must be fulfilled for voltage rating 0 – 500 kVA: frequency difference ≤0.3 Hz, RMS voltage difference ≤10% from the nominal rate, and Phase angle difference ≤20°. Short-term flicker (≤600 s) emission should be less than 0.35 and long-term (≤2 h) emission ≤0.25. The individual odd harmonic order (h) <11 is less than 4.0 %. Furthermore, transient overvoltage limits (maximum overshoot) at 0-1.6 ms is ≤2 pu, at 1.6 - 3 ms is ≤1.7 pu, at 3-16 ms is ≤1.4 pu, and at 16-166 ms is ≤1.3 pu. The power quality analysis in the presented case is based on some requirements in these recommendations.

Fig. 8-13 show the curve comparisons of the simulation results from three methods with the system parameters in Table 1. The results and discussion only present the sub-systems with LC filter due to the limited space. Nevertheless, the result of the sub-system with the LCL filter was similar in overall. The nominal frequency is 50 Hz, and the RMS voltage reference is 220 V. The impedance line of Sub-system 1 is the dominant inductive line, while Sub-system 2 is the dominant resistive line. The figures present the power quality in non-sharing (0-2 s, 10-12 s) and sharing (2-10 s) mode. The CDC method is the conventional method developed to be applicable for the dominant resistive impedance line, with the mathematic model: $\omega_{in} = \omega_r + m_i \Delta Q_i$ for angular frequency related to the reactive power and $V_{in} = V_r - m_i \Delta P_i$ for the voltage related to the active power [8]–[13]. This model improved the more conventional method presented in [7], which is more suitable for a system with the dominant inductive line impedance during power-sharing but not to the modern microgrid system where the grid tends to be resistive especially when it is in a stand-alone mode. The more improvement was to add robustness to the CDC method (called as CDC-robust in the following text) in order to have more accurate power-sharing, the steady-state condition, and add gain (K_e) were involved in the voltage control: $n_i P_i = K_e (V_r - V_o)$ [12]. These two previous methods have different structures depending upon line impedance, which is dominant in the system.

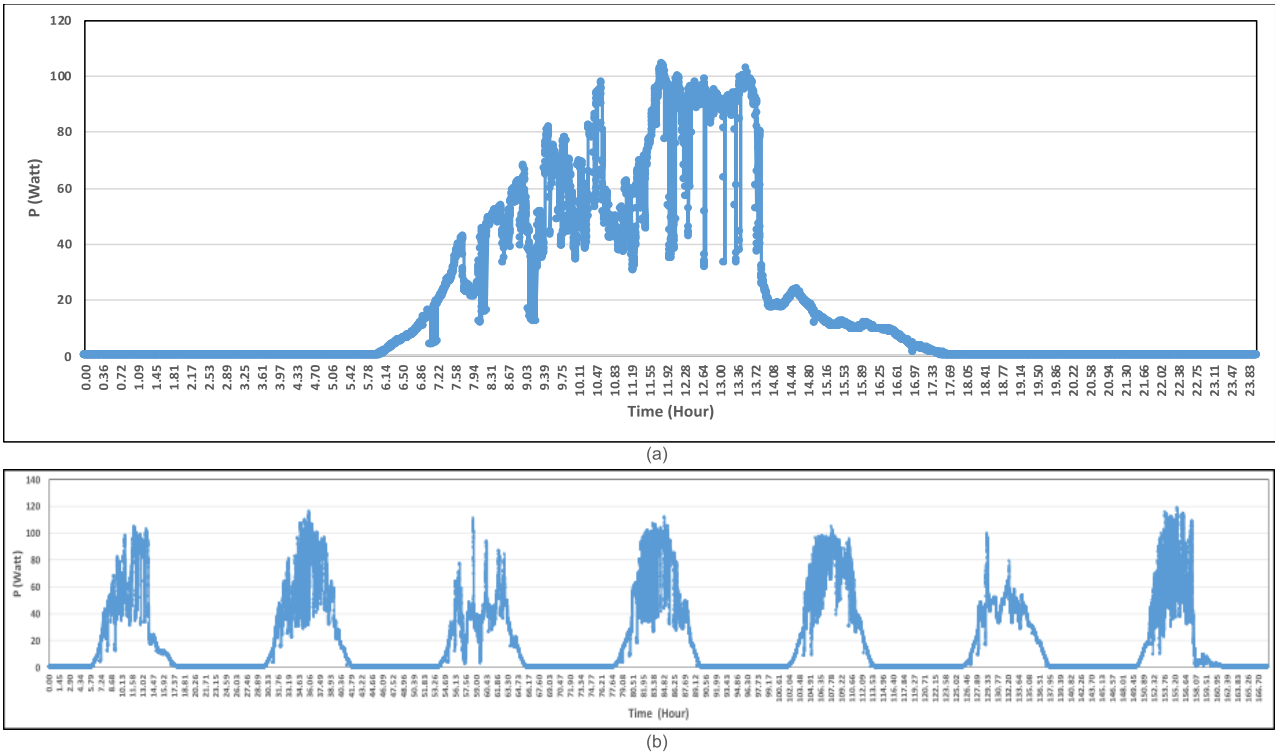

FIGURE 7. Power generated from one solar panel based on V and I data measured by IoT-based sensor in Pontianak city: (a) 7 days (168 hours), (b) the first day (24 hours).

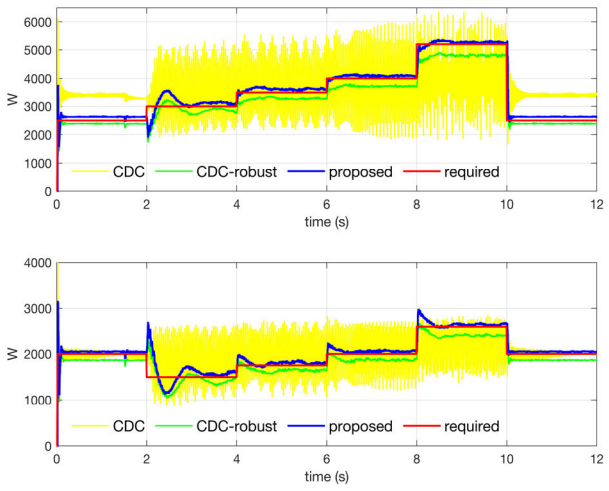

FIGURE 8. Comparison of active power (*P*) at the output terminal of sub-system 1 (top) and sub-system 2 (bottom).

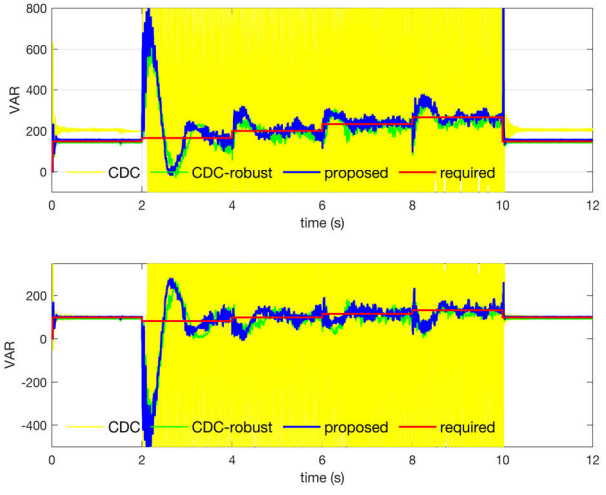

FIGURE 9. Comparison of reactive power (*Q*) at the output terminal of sub-system 1 (top) and sub-system 2 (bottom).

The proposed method can work properly, even when two sub-systems has a different type of line impedance. It is also suitable if the sub-system is not dominant to only one type, such as the type of a line impedance is resistive and inductive without the dominant one.

The relevant active power (*P*) curves in Fig. 8 shows that the CDC method is not entirely applicable for sharing mode, especially when the line impedances are different. It produces lousy curves, especially when the sharing mode is applied. The sharing quality of this method is not decent, either even the impedance lines are the same. The proposed method shows more accurate in an active power-sharing than the other two methods, once we compare them to the required power-sharing proportion (red line). A similar feature appeared for reactive power (*Q*) shown in Fig. 9. By zooming in the CDC-robust and the proposed method results, their reactive power curves have been nearly accurate to the required proportion, where reactive power of

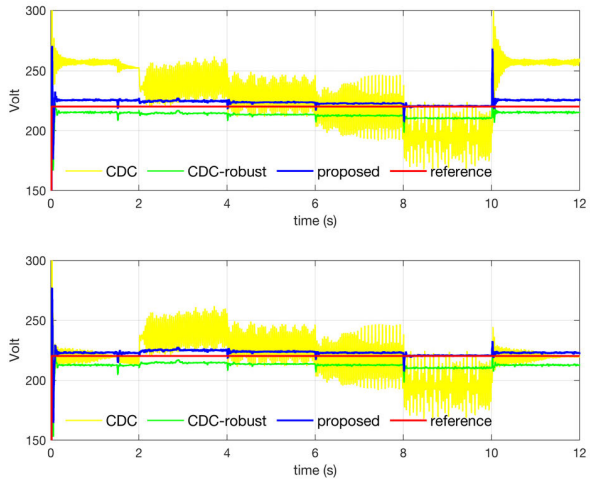

FIGURE 10. Comparison of grid RMS voltage (v_{grid}) of sub-system 1 (top) and sub-system 2 (bottom).

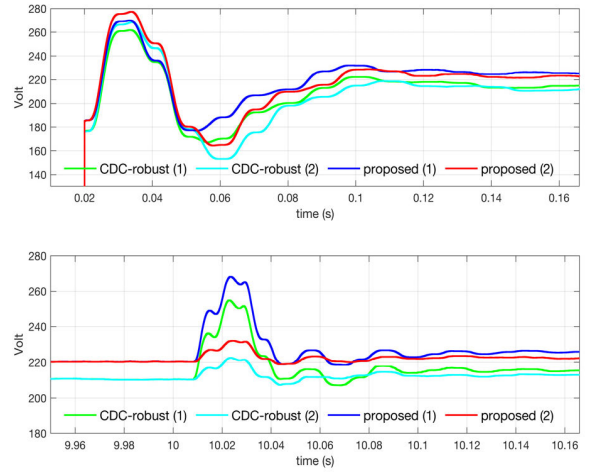

FIGURE 11. The most dynamics grid RMS voltage overshoots: around 0s when the sub-systems started to run (top) and around 10 s when the sub-systems (bottom) disconnected from the sharing mode.

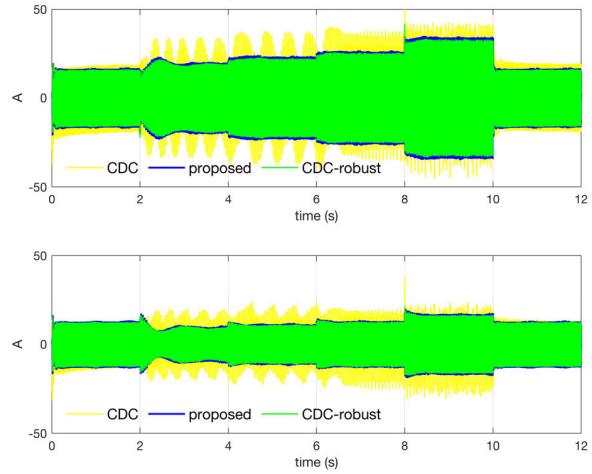

FIGURE 12. Comparison of grid current (I_{grid}) of sub-system 1 (top) and sub-system 2 (bottom).

sub-system 1 doubled than sub-system 2 in sharing mode (2 - 10 s).

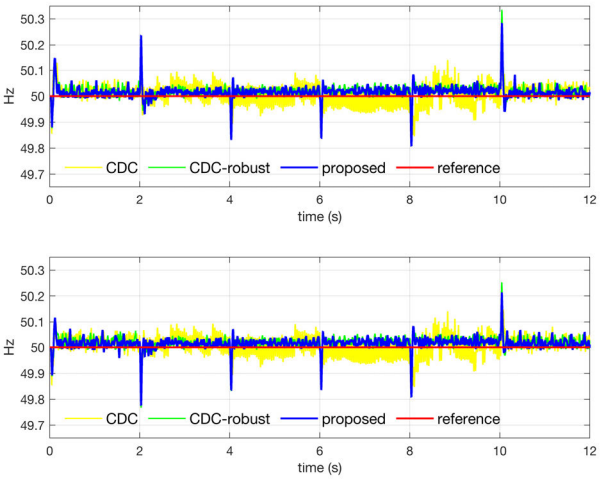

FIGURE 13. Comparison of Frequency at the output terminal (f_{grid}) of sub-system 1 (top) and sub-system 2 (bottom).

Grid terminal voltage like PCC should be maintained to have a small deviation with the RMS voltage reference (i.e., 220 V). Fig. 10 presents that the proposed method can regulate the grid RMS voltage, better than the other two methods. There are some overshoots once the sub-system is connected or disconnected to other loads, or when it changes from sharing mode to non-sharing mode and vice versa. In the figure, the highest overshoot in transient is on two points: 1) around 0 s (when the system just started) and 2) around 10 s when the system changed from sharing mode, where all loads are connected, to non-sharing mode, where sub-system 1 disconnected Load 1.1, 1.2 and 1.3, and sub-system 2 disconnected Load 2.1, 2.2 and 2.3. As shown in Fig. 11, the zoomed-in curves of these transients focused on only CDC-robust and the proposed method because the CDC shows poor quality. In the curves, the maximum overshoots (over-voltage) of the transients are still in the range mentioned before (0 – 166 ms) according to IEEE 1547 [1], in which the proposed method reveals better results since it has less deviation with the set point. The settling time due to the connection or disconnection is also acceptable during the transient on connecting and disconnecting the loads.

Furthermore, Fig. 12 depicts the grid current waveform during power-sharing and non-sharing scenarios. The CDC method shows inconvenient results with more fluctuations, while either CDC-robust and the proposed method give more stable results with a slightly different value.

Frequency needs to fulfill the required limit of deviation to its set point, i.e., 50 Hz (Indonesia electricity standard). Fig. 13 presents the related frequency curves on the grid connection, such as PCC. All presented methods could fulfill the deviation standard requirement (i.e., 0.3 Hz). There were spikes during connection and disconnection, but they are still acceptable. The CDC results show continuously higher deviations during power-sharing compared to the other two methods.

TABLE 2. Performance comparison of the system with LC filter.

Performance	CDC	CDC-robust	Proposed Method	Required
RMSE P_1 (W)	1,088.70	295.52	208.59	smaller
RMSE P_2 (W)	425.51	174.41	144.30	smaller
RMSE Q_1 (VAR)	509.35	77.87	87.67	smaller
RMSE Q_2 (VAR)	508.16	77.48	83.24	smaller
RMSE fgrid_1 (Hz)	0.0385	0.0327	0.0304	≤ 0.3
RMSE fgrid_2 (Hz)	0.0375	0.0313	0.0288	≤ 0.3
RMSE Vgrid_1 (V)	27.30	7.38	5.04	≤ 11
RMSE Vgrid_2 (V)	17.53	8.22	4.21	≤ 11
THD Vgrid_1 (%)	3.511	2.108	2.443	≤ 3
THD Vgrid_2 (%)	2.199	1.886	2.326	≤ 3
THD Igrid_1 (%)	3.505	2.906	2.449	≤ 4
THD Igrid_2 (%)	2.215	1.885	2.347	≤ 4

More performance analysis of the curves for the sub-systems applied LC filter is in Table 2. In general, the proposed method shows a better performance, although there is one parameter (i.e., Q1) with slightly lower performance than CDC-robust, they fulfill the requirements much better as a whole system. In terms of Root Mean Square Error (RMSE) between the actual active power (P1 and P2) and the desired active power-sharing, the proposed method shows more accurate power-sharing overall with significant value, while for reactive power-sharing, the RMSE values are slightly higher than the CDC-robust. For the other performance indicators, the proposed method shows better results than the other two methods. From the curves and tabulation analysis above, the proposed method shows better results in overall during the sharing and non-sharing mode. The overall results of the system using LCL filter were similar.

V. CONCLUSION

A new control method to deal with accurate power-sharing and high-power quality based on the requirements has been described in this paper. This method works mainly for sub-systems (i.e., MGS) that operate inverters in parallel. The simulation results compared CDC, CDC with robustness, and the proposed method, show that the proposed one has better results in overall performances, either in power-sharing or non-sharing mechanisms, including transient during connection and disconnection. The references for grid voltage deviation/THD, current deviation/THD, and frequency deviation were based on the IEEE recommendation (IEEE 1547). For a case study, two inverters have been considered, where each located in different sub-systems. Both can work in parallel or independent depending on the circuit breaker status. They have to supply the local loads either in sub-system 1 or 2, according to connection and disconnection scenarios. One of the advantages of the proposed method is its flexibly use in different line impedances without changing the control structure, while the other two methods, the droop control structure must be modified depending on the dominant type of impedance. The proposed method also offers the flexibility to determine various power-sharing proportions by considering the capacity of the power source as the constraint.

ACKNOWLEDGMENT

The authors thank Prof. Matthew C. Turner who just moves from the University of Leicester to University Southampton UK for his partnership and the fruitful discussion to improve the contents of the paper during the visiting in the Department of Engineering University of Leicester. They also thank to Department of Electrical Engineering, Universitas Tanjungpura, that had been facilitated the research by providing workspace, some research materials/tools, and references.

REFERENCES

[1] *IEEE Standard for Interconnection and Interoperability of Distributed Energy Resources With Associated Electric Power Systems Interfaces*, IEEE Standards Coordinating Committee 21, IEEE Standard 1547 (revision of IEEE Standard 2003), 2018.

[2] Y. Sun, C. Zhong, X. Hou, J. Yang, H. Han, and J. M. Guerrero, "Distributed cooperative synchronization strategy for multi-bus microgrids," *Int. J. Electr. Power Energy Syst.*, vol. 86, pp. 18–28, Mar. 2017.

[3] Y. Han, P. Shen, X. Zhao, and J. M. Guerrero, "An enhanced power sharing scheme for voltage unbalance and harmonics compensation in an islanded AC microgrid," *IEEE Trans. Energy Convers.*, vol. 31, no. 3, pp. 1037–1050, Sep. 2016.

[4] H. Mahmood, D. Michaelson, and J. Jiang, "Accurate reactive power sharing in an islanded microgrid using adaptive virtual impedances," *IEEE Trans. Power Electron.*, vol. 30, no. 3, pp. 1605–1617, Mar. 2015.

[5] M. M. A. Abdelaziz, M. F. Shaaban, H. E. Farag, and E. F. El-Saadany, "A multistage centralized control scheme for islanded microgrids with PEVs," *IEEE Trans. Sustain. Energy*, vol. 5, no. 3, pp. 927–937, Jul. 2014.

[6] T. Caldognetto and P. Tenti, "Microgrids operation based on master–slave cooperative control," *IEEE J. Emerg. Sel. Topics Power Electron.*, vol. 2, no. 4, pp. 1081–1088, Dec. 2014.

[7] M. C. Chandorkar, D. M. Divan, and R. Adapa, "Control of parallel connected inverters in standalone AC supply systems," *IEEE Trans. Ind. Appl.*, vol. 29, no. 1, pp. 136–143, Jan. 1993.

[8] A. Tuladhar, H. Jin, T. Unger, and K. Mauch, "Control of parallel inverters in distributed AC power systems with consideration of line impedance effect," *IEEE Trans. Ind. Appl.*, vol. 36, no. 1, pp. 131–138, 2000.

[9] J. M. Guerrero, J. Matas, L. Garcia de Vicuna, M. Castilla, and J. Miret, "Decentralized control for parallel operation of distributed generation inverters using resistive output impedance," *IEEE Trans. Ind. Electron.*, vol. 54, no. 2, pp. 994–1004, Apr. 2007.

[10] X. Yu, A. M. Khambadkone, H. Wang, and S. T. S. Terence, "Control of parallel-connected power converters for low-voltage microgrid—Part I: A hybrid control architecture," *IEEE Trans. Power Electron.*, vol. 25, no. 12, pp. 2962–2970, Dec. 2010.

[11] Q.-C. Zhong, "Robust droop controller for accurate proportional load sharing among inverters operated in parallel," *IEEE Trans. Ind. Electron.*, vol. 60, no. 4, pp. 1281–1290, Apr. 2013.

[12] Q. C. Zhong and T. Hornik, *Control of Power Inverters in Renewable Energy and Smart Grid Integration*. Hoboken, NJ, USA: Wiley, 2013.

[13] Q.-C. Zhong and Y. Zeng, "Universal droop control of inverters with different types of output impedance," *IEEE Access*, vol. 4, pp. 702–712, 2016.

[14] H. Bevrani and S. Shokoohi, "An intelligent droop control for simultaneous voltage and frequency regulation in islanded microgrids," *IEEE Trans. Smart Grid*, vol. 4, no. 3, pp. 1505–1513, Sep. 2013.

[15] J. M. Guerrero, L. GarciadeVicuna, J. Matas, M. Castilla, and J. Miret, "Output impedance design of parallel-connected UPS inverters with wireless load-sharing control," *IEEE Trans. Ind. Electron.*, vol. 52, no. 4, pp. 1126–1135, Aug. 2005.

[16] Y. Wei Li and C.-N. Kao, "An accurate power control strategy for power-electronics-interfaced distributed generation units operating in a low-voltage multibus microgrid," *IEEE Trans. Power Electron.*, vol. 24, no. 12, pp. 2977–2988, Dec. 2009.

[17] J. M. Guerrero, J. C. Vasquez, J. Matas, L. García de Vicuna, and M. Castilla, "Hierarchical control of droop-controlled AC and DC microgrids—A general approach toward standardization," *IEEE Trans. Ind. Electron.*, vol. 58, no. 1, pp. 158–172, Jan. 2011.
[18] W. Yao, M. Chen, J. Matas, J. M. Guerrero, and Z.-M. Qian, "Design and analysis of the droop control method for parallel inverters considering the impact of the complex impedance on the power sharing," *IEEE Trans. Ind. Electron.*, vol. 58, no. 2, pp. 576–588, Feb. 2011.
[19] J. He and Y. W. Li, "Analysis, design, and implementation of virtual impedance for power electronics interfaced distributed generation," *IEEE Trans. Ind. Appl.*, vol. 47, no. 6, pp. 2525–2538, Nov. 2011.
[20] J. Zhang, J. Ning, L. Huang, H. Wang, and J. Shu, "Adaptive droop control for accurate power sharing in islanded microgrid using virtual impedance," in *Proc. 43rd Annu. Conf. IEEE Ind. Electron. Soc. (IECON)*, Beijing, China, Oct. 2017, pp. 2383–2388.
[21] P. Yang, M. Yu, Q. Wu, N. Hatziargyriou, Y. Xia, and W. Wei, "Decentralized bidirectional voltage supporting control for multi-mode hybrid AC/DC microgrid," *IEEE Trans. Smart Grid*, vol. 11, no. 3, pp. 2615–2626, May 2020.
[22] K. De Brabandere, B. Bolsens, J. Van den Keybus, A. Woyte, J. Driesen, and R. Belmans, "A voltage and frequency droop control method for parallel inverters," *IEEE Trans. Power Electron.*, vol. 22, no. 4, pp. 1107–1115, Jul. 2007.
[23] X. Hou, Y. Sun, W. Yuan, H. Han, C. Zhong, and J. M. Guerrero, "Conventional P-ω/QV droop control in highly resistive line of low-voltage converter-based AC microgrid," *Energies*, vol. 9, pp. 1–19, Nov. 2016.
[24] H. Han, X. Hou, J. Yang, J. Wu, M. Su, and J. M. Guerrero, "Review of power sharing control strategies for islanding operation of AC microgrids," *IEEE Trans. Smart Grid*, vol. 7, no. 1, pp. 200–215, Jan. 2016.
[25] S. D. Panjaitan, R. Kurnianto, B. W. Sanjaya, and M. C. Turner, "Control of parallel inverters for high power quality and sharing accuracy in single-phase AC microgrids," in *Proc. 12th Int. Conf. Control (CONTROL)*, Sep. 2018, pp. 50–55, doi: 10.1109/CONTROL.2018.8516761.
[26] S. D. Panjaitan, R. Kurnianto, B. W. Sanjaya, and M. C. Turner, "DC source-based stand-alone microgrid control using I-PD scheme for a MIMO system," in *Proc. Int. Conf. Smart Cities, Autom. Intell. Comput. Syst. (ICON-SONICS)*, Yogyakarta, Asia, Nov. 2017, pp. 18–23.
[27] S. D. Panjaitan, R. Kurnianto, B. W. Sanjaya, and M. C. Turner, "I-PD control design and analysis in an islanded microgrid system," *Int. J. Smart Sens. Intell. Syst.*, vol. 10, no. 4, pp. 935–954, Dec. 2017.
[28] S. D. Panjaitan, B. W. Sanjaya, and R. Kurnianto, "Fuzzy-IP controller for voltage regulation in a stand-alone microgrid system," *Int. Rev. Autom. Control*, vol. 11, no. 3, pp. 143–150, May 2018.
[29] M. Farrokhabadi *et al.*, "Microgrid stability definitions, analysis, and examples," *IEEE Trans. Power Syst.*, vol. 35, no. 1, pp. 13–29, Jan. 2020.

SENO DARMAWAN PANJAITAN (Member, IEEE) was born in Pontianak, Indonesia, in 1975. He received the S.T. (Bachelor) degree in electrical engineering from the Universitas Tanjungpura (UNTAN), in 1997, the Pontianak-Indonesia M.T. (Master) degree in electrical engineering from the Institut Teknologi Bandung (ITB), in 2001, and the Dr.-Ing. degree in electrical and computer engineering from TU Kaiserslautern, in 2007.

From 2001 to 2006, he was a Lecturer in electrical engineering with UNTAN. From 2007 to 2009, he was a Senior Lecturer in electrical engineering with UNTAN. Since 2010, he has been an Associate Professor of electrical engineering with UNTAN. He is the author of one book and more than 20 articles. His research interests include industrial automation systems, integrated energy resources, smart energy systems, and building energy. He is an IEEE Professional Member and joining the IEEE Robotics and Automation, the IEEE Control Systems, the IEEE Power and Energy Society, and the IEEE Smart Grid Communities.

RUDI KURNIANTO was born in Pontianak, in May 1967. He received the bachelor's degree in electrical engineering from the Universitas Tanjungpura (UNTAN), in 1994, the master's degree in electrical engineering from the Institut Teknologi Bandung (ITB), in 1998, and the Ph.D. degree from the Toyohashi University of Technology, in March 2008. Since November 2008, he has been an Associate Professor with the High Voltage Engineering Group, UNTAN. His research interests include high-voltage engineering and power systems.

BOMO WIBOWO SANJAYA was born in Pontianak, in April 1974. He received the bachelor's degree in electrical engineering from the Universitas Tanjungpura (UNTAN), in 2008, and the master's and Ph.D. degrees in control engineering from the School of Electrical Engineering and Informatics, Institut Teknologi Bandung (ITB), in 2003 and 2014, respectively. He is currently a Senior Lecturer with the Department of Electrical Engineering, UNTAN. His current research interests include fuzzy logic, neural networks, and control of nonlinear dynamical systems.